High-resolution sea surface reconstructions off Cape Hatteras over the last 10 ka

C. Cléroux, Maxime Debret, Elsa Cortijo, J.C. Duplessy, F. Dewilde, J. Reijmer, Nicolas Massei

High-resolution sea surface reconstructions off Cape Hatteras over the last 10 ka

Caroline Cléroux,[1,2] Maxime Debret,[3] Elsa Cortijo,[1] Jean-Claude Duplessy,[1] Fabien Dewilde,[1] John Reijmer,[4] and Nicolas Massei[3]

Received 8 June 2011; revised 6 December 2011; accepted 6 December 2011; published 9 February 2012.

[1] This study presents high-resolution foraminiferal-based sea surface temperature, sea surface salinity and upper water column stratification reconstructions off Cape Hatteras, a region sensitive to atmospheric and thermohaline circulation changes associated with the Gulf Stream. We focus on the last 10,000 years (10 ka) to study the surface hydrology changes under our current climate conditions and discuss the centennial to millennial time scale variability. We observed opposite evolutions between the conditions off Cape Hatteras and those south of Iceland, known today for the North Atlantic Oscillation pattern. We interpret the temperature and salinity changes in both regions as co-variation of activities of the subtropical and subpolar gyres. Around 8.3 ka and 5.2–3.5 ka, positive salinity anomalies are reconstructed off Cape Hatteras. We demonstrate, for the 5.2–3.5 ka period, that the salinity increase was caused by the cessation of the low salinity surface flow coming from the north. A northward displacement of the Gulf Stream, blocking the southbound low-salinity flow, concomitant to a reduced Meridional Overturning Circulation is the most likely scenario. Finally, wavelet transform analysis revealed a 1000-year period pacing the $\delta^{18}O$ signal over the early Holocene. This 1000-year frequency band is significantly coherent with the 1000-year frequency band of Total Solar Irradiance (TSI) between 9.5 ka and 7 ka and both signals are in phase over the rest of the studied period.

Citation: Cléroux, C., M. Debret, E. Cortijo, J.-C. Duplessy, F. Dewilde, J. Reijmer, and N. Massei (2012), High-resolution sea surface reconstructions off Cape Hatteras over the last 10 ka, *Paleoceanography*, *27*, PA1205, doi:10.1029/2011PA002184.

1. Introduction

[2] The last decade of paleoclimate research has shown that the Holocene is not the stable, climatic event-free period as previously thought: both external and internal (oceanic) forcings have caused major climatic changes. Abrupt events such as the 8.2 ka event [*Alley et al.*, 1997] or the end of the African Humid Period [*deMenocal et al.*, 2000], periodic variability like the 1500 years Bond's cycle [*Bond et al.*, 1997] or the large shifts in Asian monsoon intensity [*Wang et al.*, 2005] demonstrate the dynamic range of Holocene climate and make this epoch a particularly interesting target of study. On a shorter time scale, observations over about the last 50 years show interannual and decadal climate change. These fluctuations probably persisted throughout the Holocene, together with centennial to millennial variability.

[3] External climate forcing across the Holocene changed with both solar insolation and, on shorter timescales, solar irradiance (sun activity). At 30°N, changes in the configuration of the earth's orbit from 10 to 0 ka resulted in a summer insolation decrease but a very weak mean annual insolation increase (+0.025 Watt/m^2 [*Laskar*, 1990; *Laskar et al.*, 2004]). On top of these orbital settings, solar irradiance varies on much shorter time scales. Its impact on Earth shows a high frequency variability of about 1 Watt/m^2 over the last 9.3 ka [*Steinhilber et al.*, 2009]. Recent events, like the Maunder Minimum (17th century), illustrated climate sensitivity to solar variation [*Waple et al.*, 2002]. On the millennial time scale, periodicities of about 2250-year, 1000-year, 550-year, 400-year or 220-year [*Debret et al.*, 2007; *Dima and Lohmann*, 2009; *Knudsen et al.*, 2009; *Rimbu et al.*, 2004; *Steinhilber et al.*, 2010] have been attributed to solar variability. Model simulation [*Swingedouw et al.*, 2011] and past reconstructions [*Knudsen et al.*, 2009; *Lohmann et al.*, 2004; *Morley et al.*, 2011] support an ocean-atmosphere mechanism amplifying the impact of small total irradiance change on the climate.

[4] The atmospheric circulation in the North Atlantic is described by the descending branch of the Hadley cell at midlatitudes and the ascending branch of the Polar cell at high

[1]Laboratoire des Sciences du Climat et de l'Environnement, CEA-CNRS-UVSQ/IPSL, Gif-sur-Yvette, France.
[2]Now at Lamont-Doherty Earth Observatory, Columbia University, Palisades, New York, USA.
[3]Laboratoire de Morphodynamique Continentale et Côtière, Département de Géologie, Université de Rouen, UMR CNRS/INSU 6143, Mont-Saint-Aignan, France.
[4]Department of Sedimentology and Marine Geology, FALW, VU University Amsterdam, Amsterdam, Netherlands.

0883-8305/12/2011PA002184

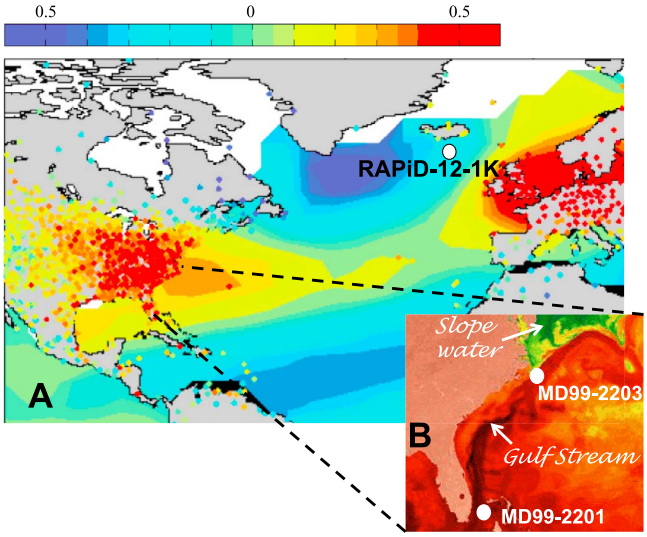

Figure 1. (a) Spatial correlation map of mean winter station temperature and sea surface temperature (SST) correlated against the NAO index. SST reflects a tripole pattern with a cold anomaly in the subpolar region, a warm anomaly in the midlatitudes region centered off Cape Hatteras, and a cold subtropical anomaly between the equator and 30°N. From *Visbeck et al.* [2001]. (b) Close-up of Cape Hatteras region, satellite image in false color. The warm Gulf Stream is seen as the dark red filament along Florida, the green color represents the cold Labrador Current (or Slope Water). Location of cores RAPiD-12-1K, MD99-2203 and MD99-2201 are plotted.

latitudes (~50°N), creating the Azores subtropical high and the Icelandic subpolar low respectively. This system oscillates in strength, and it has been well known since the first 18th century explorations that Europe and Greenland winter conditions evolve like a seesaw [*Stephenson et al.*, 2003]. The modern conceptualization of this climate pattern is the North Atlantic Oscillation (NAO) [*Hurrell et al.*, 2003] (Figure 1). Reconstruction as far back as the 16th century defines the NAO as a mode of multidecadal variability [*Gray et al.*, 2004], but NAO-like variability may also occur on centennial-millennial timescales [*Rimbu et al.*, 2003]. For NAO-like variability to occur on longer timescales, an interplay between the thermohaline circulation (THC) [*Latif et al.*, 2006], sea surface temperature (SST), and the wind-driven ocean circulation must take place [*Marshall et al.*, 2001].

[5] Our study focuses on the Gulf Stream region; this current has a wind-driven component and, as the return flow for deep-water production in the North Atlantic, it is also part of the Global conveyor belt [*Schmitz and McCartney*, 1993]. In the Gulf Stream region, model reanalysis of climate data [*Halliwell*, 1998], and satellite observations [*Kelly and Dong*, 2004] show that SST variability is associated with circulation anomalies of the wind-driven subtropical gyre (STG). When the STG is strong, heat anomalies are transported into the Gulf Stream current. This is consistent with a warming of the Gulf Stream region when the atmospheric pressure gradient between the Azores High and Iceland Low is large (NAO+, enhanced Westerlies and Trades winds), and a cooling when the pressure gradient is reduced (NAO−, weakened wind circulation) [*Frankignoul et al.*, 2001]. The STG and the subpolar gyre (SPG) are both affected by the basin-scale atmospheric circulation. Using long records of hydrographic observations from the Labrador Sea Basin and Bermuda, *Curry and McCartney* [2001] demonstrated that the pressure difference between the subtropical and subpolar gyre centers is an oceanic analogue for the NAO atmospheric pressure. Circulations within the gyres are alternatively weakened and strengthened between the NAO+ and NAO− periods. Looking at observations and model results for the northeastern Atlantic region, *Hatun et al.* [2005] concluded that SPG circulation controls both the salinity and the strength of the North Atlantic current in this region, both of which are important for deep-water formation. Indeed, both *Böning et al.* [2006] and *Gao and Yu* [2008] used model experiments to show a tight link between the SPG circulation and the strength of the meridional overturning circulation (MOC). It is worth noting that many studies that look at the relationship between the Gulf Stream and atmospheric circulation have related the Gulf Stream position (north/south displacement) with the NAO [*de Coëtlogon et al.*, 2006]. This link reflects the changes in the shape of the STG that occur under different wind regimes [*Lohmann et al.*, 2009]. Interdecadal and millennial climate variability may result from complex interactions between gyre circulation, atmospheric forcing, Gulf Stream anomaly transport and thermohaline circulation [*Dong and Sutton*, 2005].

[6] In this paper, we present temperature and salinity reconstructions off Cape Hatteras (North Carolina, USA) that cover the last 10 ka and discuss variability at the centennial-millennial time scale. We combined trace element and oxygen isotopic composition analyses on two planktonic foraminifera species to estimate past SST, past surface seawater oxygen isotopic values (a proxy for salinity) and upper thermocline conditions. We performed wavelet analysis on high-resolution surface reconstructions to find the periodicity embedded in our signals. In the discussion, we first compare our results with northeastern Atlantic climate reconstructions and evaluate NAO-like patterns. Second, we compare the paleo-hydrology off Cape Hatteras with a past reconstruction from a Great Bahamas Bank core, which represents the 'pure' Gulf Stream signal, and discuss the possible link with large-scale currents or MOC changes. Finally, we discuss the periodicities highlighted by the wavelet analysis and suggest a solar origin.

2. Materials and Methods

[7] The 38 m-long core MD99-2203 was retrieved off Cape Hatteras (34°58′38N, 75°12′06W) at 620 m water depth during the R/V *Marion Dufresne* leg MD114 of the IMAGES program (International Marine past Global Changes Study). The depth of the core minimizes any dissolution effects on the stable isotope or trace element composition of the foraminiferal tests.

2.1. Chronology, Stable Isotope and Trace Element Analyses

[8] The stratigraphy of the core MD99-2203 is based on 19 accelerator mass spectrometry ^{14}C dates measured on mixed *Globigerinoides* species (Table 1 and Figure 2). We

Table 1. Radiocarbon Dates and Calibrated Ages

Depth in Core (cm)	Corrected Depth (cm)	Radiocarbon Age BP and Error	CALIB 5 2 sigma			Age Cal Mean BP ka	Error	Lab/Year
			Age Sup BP	Age Inf BP	Age Mean BP			
101	101	1065 ± 25	676	559	618	0.62	0.06	Kiel
120	120	1445 ± 30	1031	915	973	0.97	0.06	Saclay 2009
155	155	1360 ± 40	998	787	893	0.89	0.11	BETA
170	170	2000 ± 30	1675	1479	1577	1.58	0.10	Saclay 2009
200	200	1880 ± 25	1507	1346	1427	1.43	0.08	Kiel
220	220	2230 ± 30	1731	1919	1825	1.83	0.09	Saclay 2009
250	245	2660 ± 50	2513	2184	2349	2.35	0.16	Saclay 2005
268	263	2800 ± 45	2691	2377	2534	2.53	0.16	Saclay 2005
387	265	2940 ± 40	2820	2641	2731	2.73	0.09	BETA
420	298	3735 ± 30	3776	3559	3668	3.67	0.11	Saclay 2009
460	336	3950 ± 40	4069	3827	3948	3.95	0.12	BETA
525	401	5575 ± 30	6063	5885	5974	5.97	0.09	Saclay 2009
565	441	6500 ± 30	7130	6913	7022	7.02	0.11	Saclay 2009
600	476	7670 ± 40	8243	8009	8126	8.13	0.12	Kiel
630	506	8260 ± 60	8976	8609	8793	8.79	0.18	Saclay 2005
703	579	9860 ± 50	10955	10587	10771	10.77	0.18	Kiel
710	586	10510 ± 40	11907	11404	11656	11.66	0.25	Saclay 2009
790	666	14360 ± 50	16997	16249	16623	16.62	0.37	Saclay 2009
826	702	19510 ± 80	22905	22382	22644	22.64	0.26	Saclay 2009

calibrated all ^{14}C dates into calendar ages B.P. with the CALIB 5 program [*Stuiver et al.*, 1998]. For a location close to the core, the Marine Reservoir Correction Database (http://calib.qub.ac.uk/marine/) gives a reservoir age of 412 years. Since this is very similar to the CALIB 5 default setting of 400 years correction, we did not modify this number. At the beginning of the core, two dates (at 120 cm and 170 cm) created age inversions. A careful inspection of the sediment gave no indication of reworking and because the two inversions are within the dating error, we therefore conclude that the sediment is in stratigraphic order. From 3.9 ka to 0.6 ka calendar age, the age model was derived by fitting the results with a second-order polynomial equation. Over this interval (3.9 - 0.6 ka), the least square method gives an error of 0.5 ka. The data point at 208 cm (3.67 ka) is largely responsible for this relatively high error. The same calculation without this data gives an error of 0.26 ka, which was used as the error for the 2.7 - 0.6 ka interval. The model age for the older part of the core (below 336 cm or 3.9 ka) is a simple linear interpolation between dated levels. This core has very high sedimentation rates, about 35 cm/1000 years for most of the Holocene and about 60 cm/1000 years for the most recent sediment (Figure 2).

[9] Geochemical analyses were performed on the two foraminifera species *Globigerinoides ruber* s.s. (white form) and *Pulleniatina obliquiloculata* picked from the 250–315 μm and 355–400 μm size fractions respectively. *G. ruber* is well known to inhabit the surface waters year-round in the Cape Hatteras region [*Deuser et al.*, 1981]. *P. obliquiloculata* is a warm water species whose bulk shell geochemical composition indicates calcification at the base of the upper thermocline, around 100 m depth [*Cléroux et al.*, 2007; *Farmer et al.*, 2007; *Steph et al.*, 2009]. For oxygen isotopic measurements ($\delta^{18}O$), about 7 specimens of *G. ruber* (2 specimens of *P. obliquiloculata*) were sonicated in methanol for 10 s, roasted under vacuum at 380°C for 45 min, and then analyzed on a Delta+ mass spectrometer equipped with an automated Kiel CARBO device for CO_2 production. Results are expressed relative to the Vienna Pee Dee belemnite standard (PDB). Long-term analytical precision of $\delta^{18}O$ measurements from standard measurements is ±0.07 ‰. Most of the *G. ruber* samples were replicated at least twice and up to six times, except in the 260–380 cm intervals where *G. ruber* abundance was low (Figure 3); the mean standard deviation of replicates is ±0.21 ‰ (Figure 3). About 9% of the *P. obliquiloculata* samples were replicated with a mean standard deviation of 0.16 ‰ (not shown).

[10] Approximately 200 μg of material were used for Mg/Ca ratio measurements, i.e., 20–30 tests of *G. ruber*, 6–8 tests of *P. obliquiloculata*. Samples were cleaned following the procedure of *Barker et al.* [2003] including: several water and ethanol rinses, hydrogen peroxide washing in a boiling water bath and finally a short (30s) dilute acid

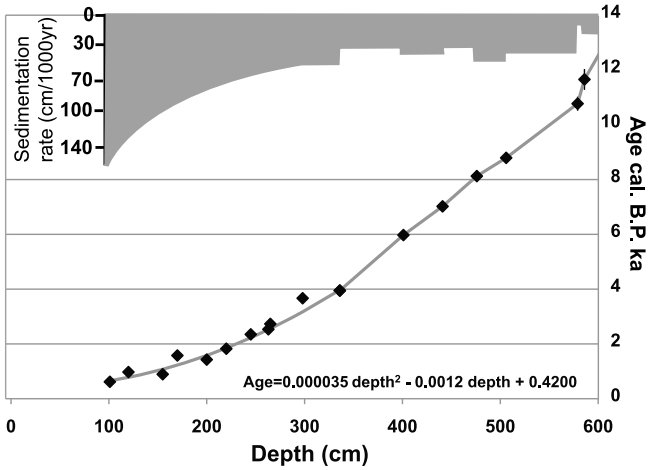

Figure 2. (top) Sedimentation rate and (bottom) age model for the core MD99-2203. From 0.6 ka to 3.9 ka, we fitted a second-degree equation between the data. The oldest part of the core is dated by linear interpolation between the data. Error bars on the calibrated ages are smaller than the size of the markers, only the uncertainty on the last date at 11.6 ka can be seen.

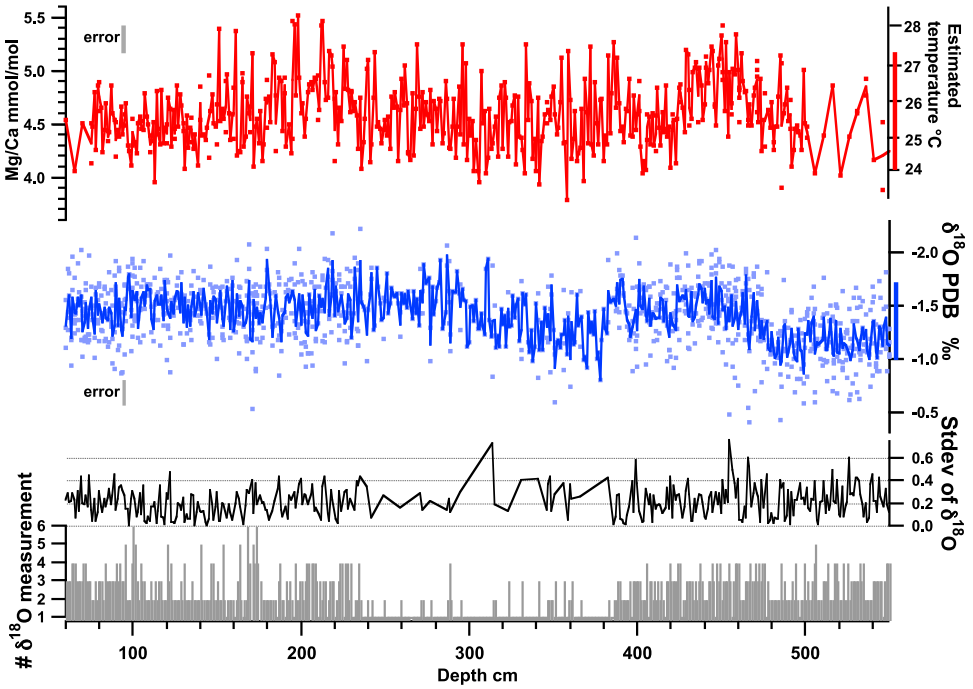

Figure 3. Mg/Ca ratio and $\delta^{18}O$ data for *G. ruber* by depth in the core for all the replicates. The bars plotted are: the error bars (gray), summer-spring surface temperature range from the World Ocean Atlas (red) and calculated $\delta^{18}O_{calcite}$ at the surface for the warm season at the core location (blue). The continuous lines are the average between replicates. The two lower panels represent the standard deviation and the number of replicates for the $\delta^{18}O$ analysis.

leaching with 0.001 M nitric acid. Prior to measurement, samples were dissolved with 350 μl of 0.075 M nitric acid, centrifuged and analyzed with a Varian Vista Pro AX simultaneous inductively coupled plasma-atomic emission spectrometer (ICP-AES) at the LSCE. Samples with Fe/Ca or Mn/Ca ratio higher than 0.1 mmol/mol were rejected. The mean standard deviation of a standard solution with a Mg/Ca ratio of 5.23 mmol/mol is 0.026 mmol/mol. 493 *G. ruber* samples were analyzed for Mg/Ca ratio among which 58 were replicates (i.e., 12%) (Figure 3). The mean standard deviation for these replicates is 0.19 mmol/mol (or 4.24% in 'residue standard deviation' or RSD). 199 *P. obliquiloculata* samples were analyzed for Mg/Ca ratio among which 40 were replicates (i.e., 20%). The mean standard deviation for these replicates is 0.24 mmol/mol (or 10.2% in RSD).

2.2. Calculation of Temperature From Mg/Ca Ratio and $\delta^{18}O_{seawater}$ Reconstruction

[11] This study exploits the now standard method of paired $\delta^{18}O$ and Mg/Ca ratio measurements on the same sample to reconstruct the temperature and the $\delta^{18}O$ of the seawater where the foraminifera calcified (i.e., calcification temperature and calcification $\delta^{18}O_{seawater}$).

[12] The foraminiferal Mg/Ca ratio is widely used as a temperature proxy [*Elderfield and Ganssen*, 2000; *Nürnberg et al.*, 1996]. Temperatures have been calculated using equations from *Cléroux et al.* [2008] for both species. These calibrations were established from North Atlantic core tops and with the same cleaning procedure for trace element analyses used in this study. Both calibration equations for the two species are in very good agreement with previously published calibrations [*Anand et al.*, 2003] but there is more calibration points for *P. obliquiloculata* in Cléroux et al.'s study than in *Anand et al.*'s [2003] study.

[13] For *G. ruber:*

$$SST(^{\circ}C) = \frac{1}{0.070}\ln\left(\frac{Mg/Ca(mmol/mol)}{0.76}\right)$$

The error associated with this calibration is 1.3°C [*Cléroux et al.*, 2008]. Over the range of Mg/Ca measured on *G. ruber* for this study (4 to 5.5 mmol/mol), this equation is almost linear and the traditional approach to calculate uncertainty is applied. The mean *G. ruber* Mg/Ca is 4.5 mmol/mol, therefore ±0.19 mmol/mol translates into 0.60°C. The uncertainty on SST reconstruction is therefore 1.4°C [$(1.3^2 + 0.6^2)^{1/2}$].

[14] For *P. obliquiloculata:*

$$T(^{\circ}C) = \frac{1}{0.039}\ln\left(\frac{Mg/Ca(mmol/mol)}{1.02}\right)$$

The error associated with this calibration is 0.8°C [*Cléroux et al.*, 2008]. The mean Mg/Ca for *P. obliquiloculata* is 2.3 mmol/mol, therefore ±0.24 mmol/mol translates into 2.7°C. Taking the linear approximation (Mg/Ca for *P. obliquiloculata* ranges between about 1.5 to 3 mmol/mol), the uncertainty on subsurface temperature reconstruction is 2.8°C [$(0.8^2 + 2.7^2)^{1/2}$].

[15] It has been recently suggested that salinity also has an effect on the Mg/Ca ratio and quantification of this effect is under development. It is still unclear whether this excess of Mg due to salinity only appears in high salinity regions [*Arbuszewski et al.*, 2010; *Ferguson et al.*, 2008] or whether

it is a persistent effect [*Mathien-Blard and Bassinot*, 2010]. Considering a very large salinity range within worldwide samples, *Mathien-Blard and Bassinot* [2010] found no effect of salinity on Mg/Ca thermometry for salinities around 35.4‰. This value is very close to the modern mean surface salinity at our core site (35.9 ± 0.2‰), giving confidence that the salinity effect on our Mg/Ca ratio is negligible.

[16] The $\delta^{18}O$ composition of foraminifera records both the oxygen isotopic composition of seawater ($\delta^{18}O_{seawater}$) and the calcification temperature (through the kinetic fractionation effect) [*Emiliani*, 1955]. Shell $\delta^{18}O$ and Mg/Ca calcification temperature values for *G. ruber* are substituted into the oxygen isotope paleotemperature equation [*Shackleton*, 1974] to solve the $\delta^{18}O_{seawater}$. We included +0.27 ‰ to account for the difference between PDB and SMOW (Standard Mean Ocean Water).

$$\delta^{18}O_{seawater}(‰) = \left(\delta^{18}O_{foram}(‰) + 0.27\right) - 5\left(4.38 - \sqrt{\left(4.38^2 - 0.4 \times \left(16.9 - T_{Mg/Ca}(^{\circ}C)\right)\right)}\right)$$

If Y = f (X_1, X_2,…, X_n), with σ_{Xi} is the standard error associated with each X_i. The following equation gives the propagated error on Y, called σ_y:

$$\sigma_Y^2 = \sum_{i=1}^{n}\left(\frac{\partial f}{\partial X_i}\right)^2 \sigma_{Xi}^2$$

with $\frac{\partial f}{\partial X_i}$ the partial derivative of f with respect to each X_i. We use this calculation of uncertainty to propagate the error in the $\delta^{18}O_{seawater}$ equation (see auxiliary material).[1] Using the full Shackleton's equation (as expressed above), the propagated uncertainty increased exponentially with temperature. It is equal to about 1‰ around 25°C, this is likely an overestimation. Over the range of temperature covered by our study, a simplified Shackleton's equation can be used and gives a propagated $\delta^{18}O_{seawater}$ uncertainty of 0.38‰ (see auxiliary material).

[17] The effect on $\delta^{18}O_{seawater}$ of global ice volume changes has been corrected [*Waelbroeck et al.*, 2002]. Note that the above uncertainty estimate does not take into account the correction for ice volume change, see *Schmidt* [1999] for ample discussion. The $\delta^{18}O_{seawater}$ equation again assumes no salinity influence on the Mg/Ca ratio. To estimate this effect, we used the $\delta^{18}O_{seawater}$ equation proposed by *Mathien-Blard and Bassinot* [2010] that includes a correction for the salinity effect on the Mg/Ca ratio. The newly calculated $\delta^{18}O_{seawater}$ only differs by a lower value of about 0.15‰ (or 0.3‰ in salinity) for the 3.5–5 ka period. Since the effect is minimal, we decided not to adopt the equation of Mathien-Blard and Bassinot because it is mainly constrained by Indo-Pacific core top data.

2.3. Oceanographic Context

[18] Core MD99-2203 was retrieved within the Gulf Stream path. This warm and salty current forms in the Gulf of Mexico and circulates northward along the Florida coast. At Cape Hatteras, it meets the cold, southward flowing Labrador Current (Figure 1). Whether it is the topography, the influence of the southward flowing Deep Western Boundary Current, or the zero-wind stress curl, the Gulf Stream leaves the U.S. coast at Cape Hatteras to continue its course across the Atlantic [*Dengg et al.*, 1996].

[19] We examined the hydrology at the MD99-2203 core site with the World Ocean Atlas (WOA 2001) [*Conkright et al.*, 2002] to extract large spatial and temporal mean conditions and with very high resolution temperature and salinity 'snapshot' profiles provided by Argo floats (http://www.ifremer.fr/WC2argoFloats/) and WOCE-UOT program (http://woce.nodc.noaa.gov/wdiu/diu_summaries/woce-uot/atl.htm) (Figure 4). WOA gives surface temperature ranging from 24°C in spring to 27.3°C in summer and year-round salinity at 35.9 ± 0.2‰ (0–30 m mean).

[20] The Argo and UOT profiles show that a very shallow low salinity surface layer covers the MD99-2203 core site: this fresh water layer comes from north of the core site, as shown by profile 166 (Figure 4). This fresh layer is not cold: all the profiles have a warm surface layer (compare for example profiles 157 and 164, Figure 4). This fresh layer represents a mixture between Labrador Current water, coastal water, and Gulf Stream water, and it is referred to as Slope Water. It was identified in early studies as low salinity, southward flowing water between the U.S. coast and the Gulf Stream [*Atkinson et al.*, 1983; *Bumpus*, 1973]. More recent works confirmed the passage of Labrador-type water south of Cape Hatteras [*Gawarkiewicz and Linder*, 2006; *Pietrafesa et al.*, 1994].

3. Results

3.1. Surface Water Reconstruction

[21] Mg/Ca ratios of *G. ruber* vary by about 0.5 mmol/mol (or about 1.5°C when converted to temperature), and $\delta^{18}O$ variability is less than 0.5‰ (Figure 3). This variability is in agreement with the warm season variability and also with inter-annual surface variability reconstructed from previous works. Using annually resolved coral analysis from the Bahamas (25.84°N, 78.62°W, along the Gulf Steam path), *Saenger et al.* [2009] reconstructed SST with an inter-annual variability of about 1.5°C over a 439-year time period. Very high resolution *G. ruber* $\delta^{18}O$ measurement from the Bahamas region and the Florida Straits over the last 2 ka show variability with a 0.4‰ amplitude [*Lund and Curry*, 2006].

[22] The $\delta^{18}O_{seawater}$ is locally related to salinity, as both quantities are affected by evaporation and precipitation. We computed the following $\delta^{18}O_{seawater}$-salinity relationship for a large region extending from the Caribbean Sea to Nova Scotia using the GISS database [*Schmidt et al.*, 1999]

$$\delta^{18}O_{seawater}(‰) = 0.42 \times Salinity(‰) - 14.23$$

Past sea surface salinity can therefore be estimated from $\delta^{18}O_{seawater}$, calculated from $\delta^{18}O_{foram}$ and $T_{Mg/Ca}$. When this relationship is applied to calculate past salinity, it is assumed that the modern relationship, defined by the covariation between the two quantities on a particular region (spatial relationship), is a good approximation for change in past $\delta^{18}O_{seawater}$ and salinity (temporal relationship). This might not be true if the evaporation-precipitation ratio in the source region changes or if moisture transport changes [*Rozanski et al.*, 1993]. So far, only models can help calculate the $\delta^{18}O_{seawater}$-salinity relationship back in time. The only attempt to estimate the past $\delta^{18}O_{seawater}$-salinity relationship shows that within the 0.5–0.9‰ range for

[1] Auxiliary materials are available in the HTML. doi:10.1029/2011PA002184.

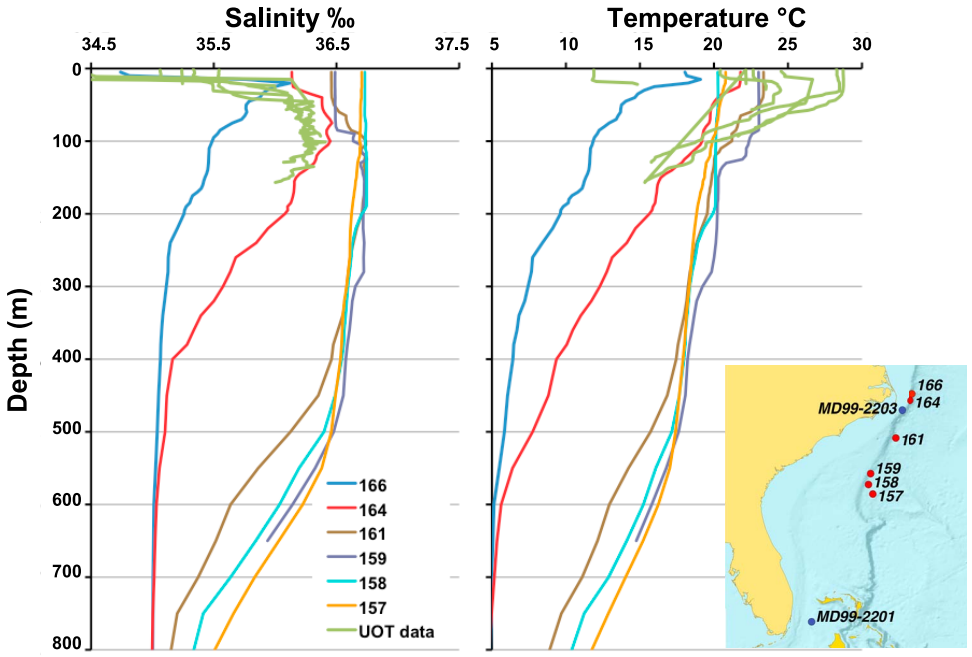

Figure 4. (left) Salinity and (right) temperature versus water depth (m) extracted from Argo station (numbered profiles) and Upper Ocean Thermal atlas (green profiles, all extracted within less than 0.25° around MD99-2203 site). Map in inset shows Argo station locations.

$\delta^{18}O_{seawater}$, the relationships for modern or Mid-Holocene are very similar [*Schmidt et al.*, 2007]. As this is the range for modern $\delta^{18}O_{seawater}$ and most of the $\delta^{18}O_{seawater}$ reconstructed in this study, we consider our salinity estimates robust. The salinity reconstructed from our data is in agreement with modern conditions at the core location (mean reconstructed salinity 35.7 ± 0.35‰, against 35.9 ± 0.2‰ from WOA).

[23] During the late Holocene (before 0.9 ka and between 2 and 3.5 ka) and near 6 ka, surface water $\delta^{18}O_{seawater}$ (salinity) reconstructed off Cape Hatteras was low (Figure 5). Periods with high surface $\delta^{18}O_{seawater}$ (salinity)

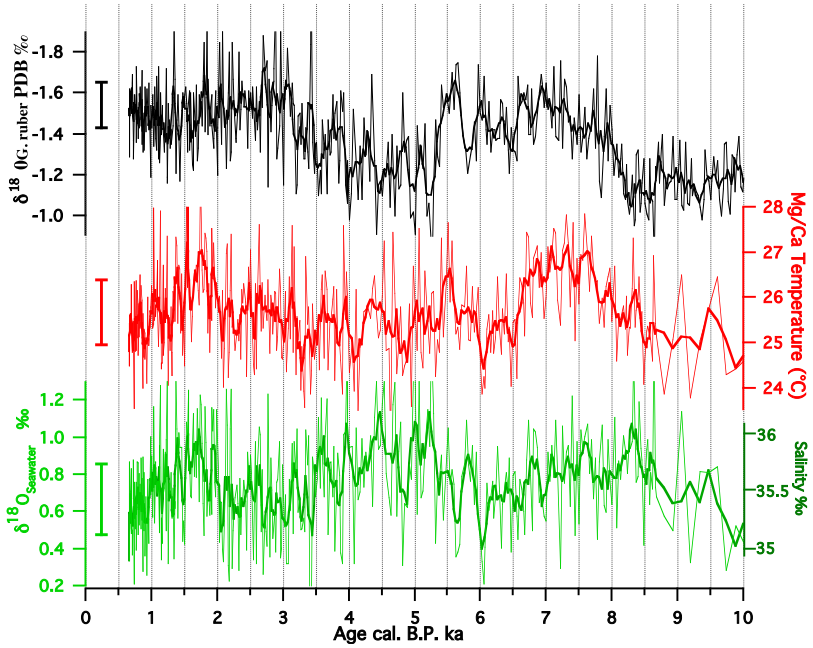

Figure 5. The $\delta^{18}O$, temperature (°C) from Mg/Ca ratio, $\delta^{18}O_{seawater}$ (corrected for ice volume changes) and estimated surface salinity for *G. ruber* of MD99-2203. Thick curves represent a 5-point smoothing. Estimated uncertainties for each data are plotted (vertical bars).

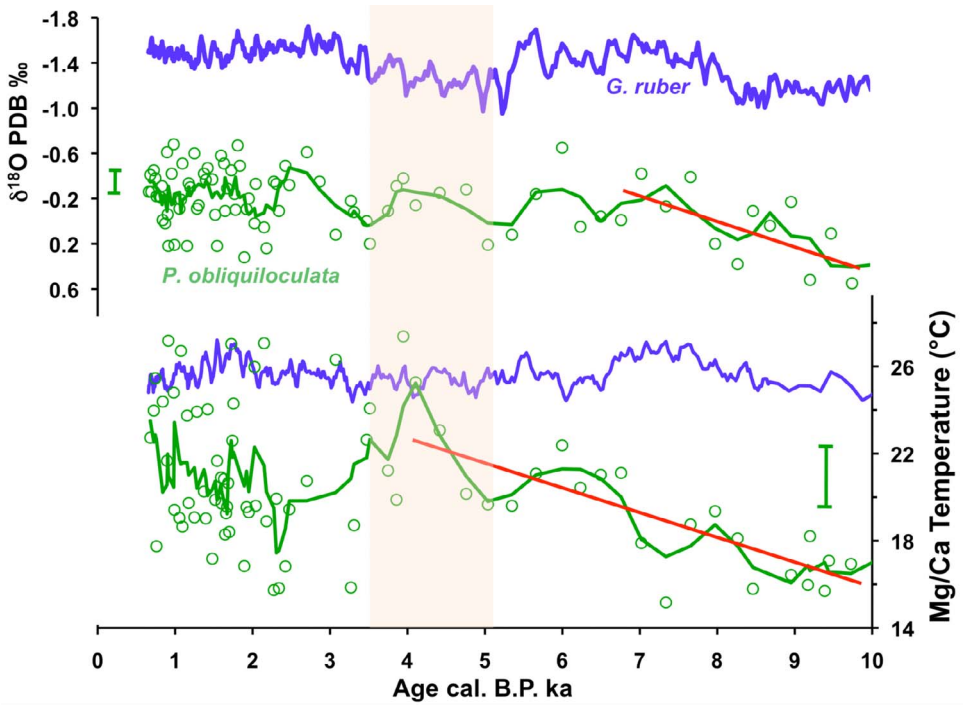

Figure 6. Comparison between *G. ruber* (blue) and *P. obliquiloculata* (green) (top) $\delta^{18}O$ and (bottom) temperature from Mg/Ca ratio. Thick green curves represent a 3-point running average. Error bars, trends (red lines) and the period of low upper water column stratification (yellow rectangle) are plotted.

occurred at 1.7 ka, from 3.5 ka to 5.2 ka, 7.6 ka, and 8.3 ka. The period between 3.5 and 5.2 ka is noticeably different with elevated $\delta^{18}O_{seawater}$ but low temperature.

3.2. Upper Thermocline Reconstruction

[24] We compared geochemical measurements between *G. ruber* and *P. obliquiloculata* to assess the state of stratification of the upper water column over the last 10 ka (Figure 6). We observe a 0.5‰ decrease in the $\delta^{18}O$ of *P. obliquiloculata* between 10 ka and 7 ka, after 7 ka no trend can be distinguished in the $\delta^{18}O$. Temperature reconstructed from Mg/Ca ratio analyses on *P. obliquiloculata* shows a warming of about 6°C from 10 ka to 4 ka. The warmest sub-surface conditions are recorded between 5 ka and 3.5 ka. After 4 ka, upper thermocline temperatures cool but are very scattered. These records contrast with the very steady $\delta^{18}O$ and SST reconstructed for the surface, and thus indicate a large water column structural change: the water column was much less stratified between 5 ka and 3.5 ka (subsurface warmer and saltier to keep a constant $\delta^{18}O$).

3.3. Wavelet Analysis on *G. ruber* Signals

[25] All *G. ruber* series (mean value of replicates), $\delta^{18}O_{foram}$, SST-Mg/Ca and $\delta^{18}O_{seawater}$, have been detrended using a second polynomial and analyzed through wavelet transform to determine periodic signals (Figure 7). Cubic spline interpolation was used to handle the uneven temporal resolution. Wavelet transform is a band-pass filter, which consists of convoluting the signal with scaled and translated forms of a highly time-localized wave function. Wavelet analysis is better suited to describe non-stationarities, i.e., discontinuities, in frequency of space through time than Fourier spectral analysis, and is sensitive to rapid events in a time series. In order to prevent the spectrum from gathering too much energy in the vicinity of the very high amplitude 5.6 ka event, the $\delta^{18}O_{foram}$ record has been cut in two parts prior to wavelet analysis (Figures 7a–7c). The wavelet analysis method underestimates the lowest frequency near the edges of the spectrum. On each plot, the energy bands outside the cone of influence (black line) are likely to appear less powerful than they actually are because edge effects are becoming important. Detailed methodology can be found in the work by *Debret et al.* [2007].

[26] The $\delta^{18}O_{foram}$ signal in the 10 to 5.8 ka time slice is well structured by a ~1000-year period. A less powerful 330-year period shows up in the most recent part of this time period, around 6.5 ka (Figure 7c). During the late Holocene (5.35–0.6 ka), the only significant frequency is found around 5 ka, representing a 256-year period.

[27] In the same way, the $T_{Mg/Ca}$ signal is well structured for the early part of the Holocene with 330-year, 1800-year and 2600-year periods, whereas the late Holocene lacks any period (Figure 7d). The $\delta^{18}O_{seawater}$, calculated from $\delta^{18}O_{foram}$ and $T_{Mg/Ca}$, presents a less structured signal (Figure 7e). As for $\delta^{18}O_{foram}$, a 250-year period appears around 5 ka.

[28] The most powerful (significant) period highlighted by this analysis is the ~1000-year period found only in the $\delta^{18}O_{foram}$ during first part of the Holocene. This 1000-year period is also interesting because it is frequently find in paleoceanographic studies. This period is not found in the SST-Mg/Ca record or in the $\delta^{18}O_{seawater}$ record although both parameters are involved in the $\delta^{18}O_{foram}$. One possible explanation is that salinity plays a large role in the $\delta^{18}O_{foram}$ signal. The larger uncertainties associated with SST-Mg/Ca

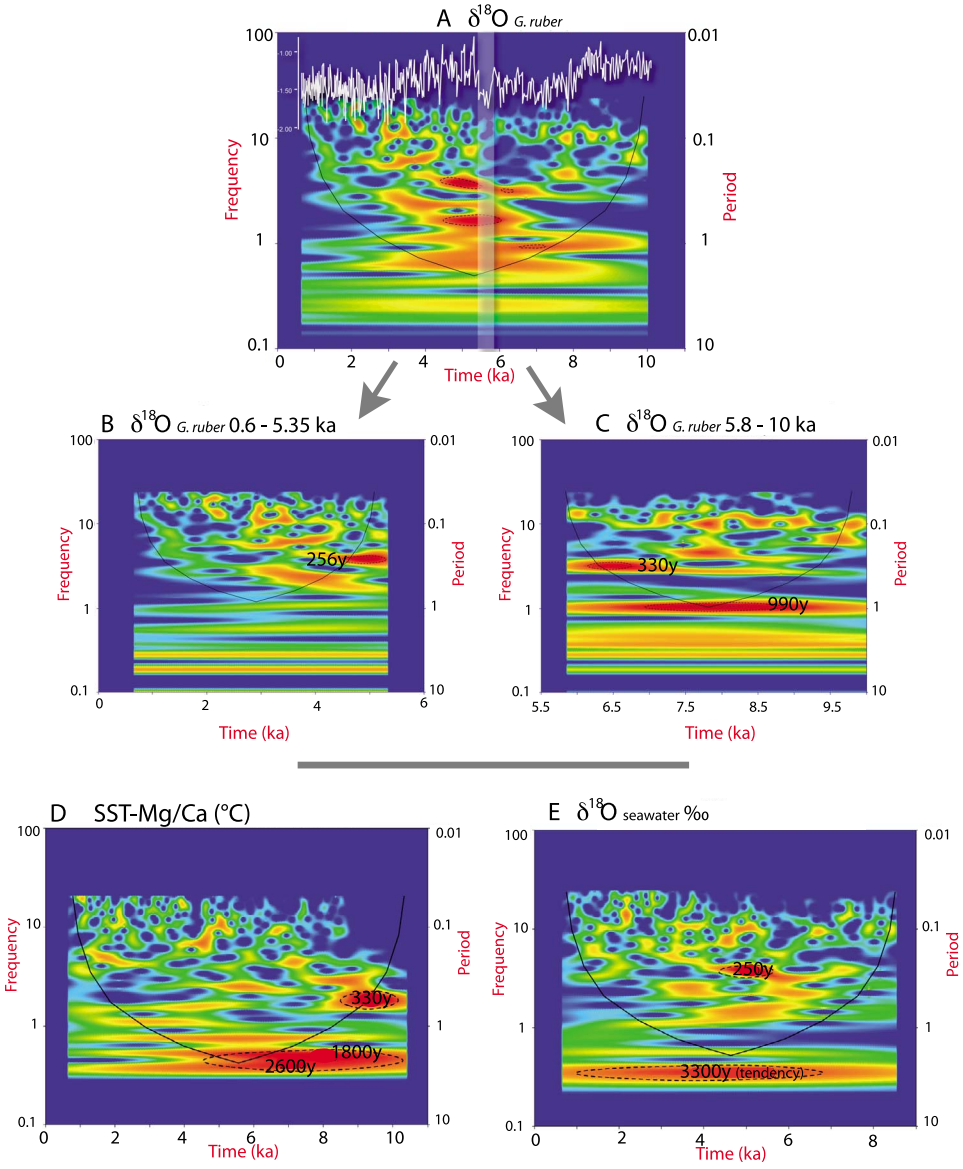

Figure 7. (a–c) Wavelet transform analysis of *G. ruber* $\delta^{18}O$, (d) temperature from Mg/Ca, and (e) seawater $\delta^{18}O$. For the analysis of $\delta^{18}O$ signal, the whole period (0.6–10 ka; Figure 7a) has been cut in two parts (Figures 7b and 7c) to avoid an artificial frequency created by the event around 5 ka. Dotted lines encompass the significant peak in the wavelet spectra, i.e., peak significant in the 95% confidence limit using Monte-Carlo simulation.

and $\delta^{18}O_{seawater}$ reconstructions may also preclude any meaningful frequency analysis.

4. Discussion

4.1. Comparison Between the Climatic Evolution of the Gulf Stream Area and the NE Atlantic Region Over the Holocene

[29] Cape Hatteras is at the center of one of the three poles defining SST anomaly associated with the NAO; the two other poles being the subpolar region and the region between the equator and 30°N [*Visbeck et al.*, 2001] (Figure 1). Mechanisms associated with the NAO generate an anti-phase between conditions in the Cape Hatteras region and the subpolar Atlantic region; when the NAO index is positive, enhanced Westerlies flowing across the North Atlantic induces colder and drier than average conditions over the northeastern Atlantic and warmer and wetter than average conditions in the eastern U.S.; and vice versa during negative NAO periods. We acknowledge that the NAO is defined as a decadal mode, but here we want to explore a possible link between the Cape Hatteras region and the NE North Atlantic over the Holocene. Numerous summer SST records from geochemical analyses on surface-dwelling planktonic foraminifera species [*Came et al.*, 2007; *Thornalley et al.*, 2009], alkenone [*Sicre et al.*, 2008], diatoms [*Birks and Koç*, 2002] or foraminifer transfer function [*Risebrobakken et al.*, 2003] are available for the NE North Atlantic.

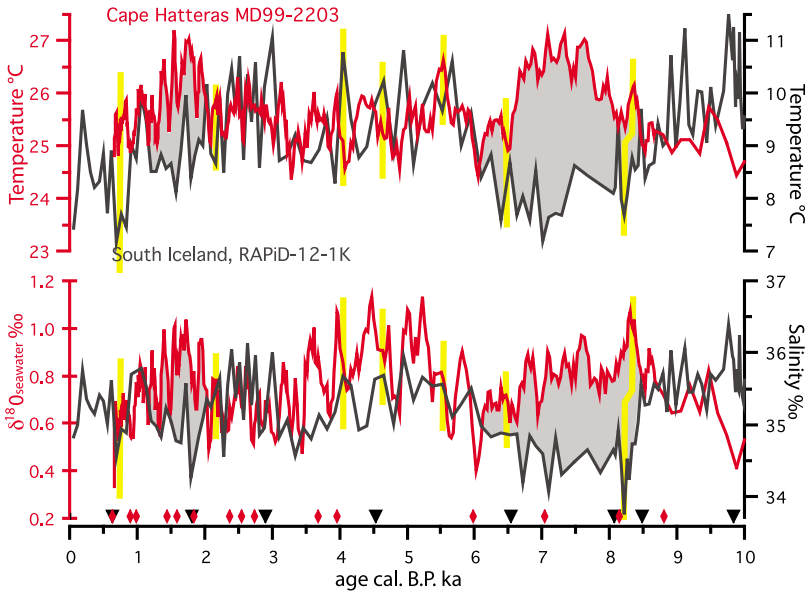

Figure 8. Comparison between Cape Hatteras (MD99-2203, red, left axis) and South Iceland (RAPiD-12-1K, black, right axis) reconstructions. (top) Temperature (in °C) reconstructions from Mg/Ca ratio; (bottom) $\delta^{18}O_{seawater}$ and salinity reconstruction from Cape Hatteras and South Iceland, respectively. Radiocarbon dates converted in calendar age for both cores are indicated on the time axis. Periods of observed anti-correlation are marked (gray area and yellow bars).

Previous compilation [see, e.g., *Andersson et al.*, 2010] showed inconsistency between phytoplankton-based and zooplankton-based reconstructions. Seasonality, habitat depth, sea-ice or local effects (for location close to the continent) bias each proxy. We chose to compare our SST and $\delta^{18}O_{seawater}$ (salinity) off Cape Hatteras with a temperature and salinity reconstruction from *Globorotalia inflata* in the RAPiD-12-1K core located south of Iceland (62°05N, 17°49W, 1938 m depth). This core, among the one with higher time resolution in the area and among the few with salinity reconstruction, is located close to the region of maximum influence of the NAO and is also influenced by the North Atlantic Current (mostly derived from the Gulf Stream). This core has been shown to be influenced by gyre variability associated with the NAO [*Thornalley et al.*, 2009]. Our choice was also largely motivated because *G. inflata* is a deep-dwelling planktonic foraminifera species representing, at this latitude, the conditions at the base of the summer thermocline [*Cléroux et al.*, 2007; *Ganssen and Kroon*, 2000]. *G. inflata* is therefore more likely to record temperature and salinity close to the annual mean, whereas surface-dwelling species are more likely to record summer conditions influenced by insolation changes [*Thornalley et al.*, 2009]. Ideally, these 'close to' subpolar mean annual surface temperature and salinity conditions should be compared with mean annual surface conditions in the Cape Hatteras region. A caveat of this study is that our MD99-2203 temperature and salinity reconstructions reflect the warm season more.

[30] Here we take a simple approach to observe the reconstructions in both regions with the intention of establishing a basic comparison with modern climatic pattern. The comparison shows two periods of temperature and salinity divergences (Figure 8). Between 8 and 6.5 ka and 2–1 ka, warm and salty conditions off Cape Hatteras contrasted with cold and fresh conditions south of Iceland. Both cores are plotted with their own age models, still many centennial scale temperature and salinity events also present an anti-phase structure between the two locations (for example around 8.2, 6.2, 5.7, 4.2 and 0.8 ka). In the vein of recent studies supporting NAO-like variability over the Holocene [*Giraudeau et al.*, 2010; *Kim et al.*, 2007; *Rimbu et al.*, 2003; *Wanner et al.*, 2008], this pattern looks like large-scale NAO-like anti-correlation. More than the atmospheric pattern, the temperature and salinity divergences between the Gulf Stream area and the Icelandic region may reflect the states of the STG and the SPG. The observation of low salinity conditions over the NE Atlantic has previously been identified as a sign for intensified SPG circulation [*Hatun et al.*, 2005]. On the other hand, SST increase in the Gulf Steam is also a sign for active STG [*Kelly and Dong*, 2004]. From this comparison, the 8–6.5 ka and 2–1 ka periods seem to have seen enhanced gyres circulation. This is consistent with the modern coupling between the SPG and the STG [*Curry et al.*, 1998]. Temperature reconstructions off North Africa [*Kim et al.*, 2007], also indicate warm STG or strong Trade wind over these periods.

[31] Our study strengthens the idea that both subpolar and subtropical gyres in the North Atlantic evolve together creating opposite temperature and salinity changes on millennial time scales, but a lot of future work is needed to confirm these observations.

4.2. Positive Surface Salinity Anomaly off Cape Hatteras: Origin and Possible Scenarios

[32] Between 5.2 and 3.5 ka and around 8.3 ka, the reconstructed surface $\delta^{18}O_{seawater}$ (salinity) off Cape Hatteras are higher compared to the average value reconstructed over the last 10 ka but temperatures are not warmer (Figure 5). In the Gulf Stream and its source region, present-

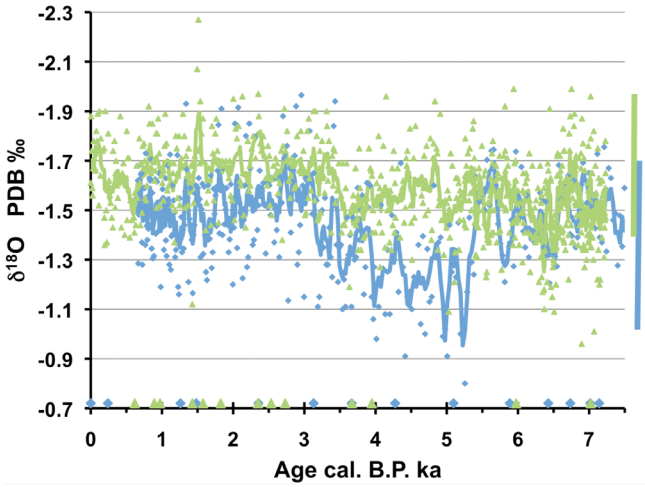

Figure 9. *G. ruber* δ^{18}O of MD99-2203 (blue) and *G. sacculifer* δ^{18}O of MD99-2201 (green) along the last 7.3 ka. Colored bars represent the spring-summer δ^{18}O expected at each core site. Radiocarbon dates converted in calendar age for both cores are indicated on the time axis.

day temperature and salinity are well correlated [*Thacker*, 2007; *Thacker and Sindlinger*, 2007], this decoupling in our record deserves discussion.

[33] The event recorded off Cape Hatteras around 8 ka is close enough to the '8.2 ka event' to suggest a link. The 8.2 ka event is a severe cooling over the North Atlantic region and over Greenland [*Alley et al.*, 1997; *Thomas et al.*, 2007]. The origin of this cooling is still widely discussed, and whether or not it implies a slowing or shut down of the thermohaline circulation is still controversial [*Keigwin et al.*, 2005; *Kleiven et al.*, 2008; *Wiersma and Renssen*, 2006]. This event has been poorly documented in the low and midlatitude Atlantic regions, and few studies indicate colder condition off Cape Ghir [*Kim et al.*, 2007] and drier conditions over North Africa and the Caribbean Sea [*Wiersma and Renssen*, 2006]. Here we report saltier conditions in the Gulf Stream area during this event.

[34] To understand the origin of the salinity increase off Cape Hatteras between 5.2 and 3.5 ka, we compared our record with a *G. sacculifer* δ^{18}O record from core MD99-2201 located within the Gulf Stream path in the Great Bahamas Bank (25°5 N, 79°1 W, 290 m depth) (Figure 9) [*Roth and Reijmer*, 2004]. This very well dated core spans the last 7.5 ka. Sediment trap studies in the Sargasso Sea show that *G. sacculifer* has a similar habitat as *G. ruber* [*Deuser and Ross*, 1989]. The δ^{18}O of *G. sacculifer* are well within the range expected for the spring and summer surface conditions at MD99-2201 site (26.6°C to 29°C, salinity around 36.17‰, δ^{18}O expected: −1.45‰ to −2‰).

[35] The two records differ markedly between 5.2 and 3.5 ka (Figure 9), i.e., when the core from off Cape Hatteras indicates surface $\delta^{18}O_{seawater}$ (salinity) increase (Figure 5) and a less stratified water column (Figure 6). Both MD99-2201 and MD99-2203 are located along the Gulf Stream path but only the MD99-2203 site is influenced by the Labrador Current / Slope Water (Figure 1). We infer that the divergence at 5.2–3.5 ka comes from this second water mass. Two mechanisms can explain the salinity increase off Cape Hatteras: 1) the Labrador Current / Slope Water was itself more salty or 2) the low-salinity Labrador Current / Slope Water was not reaching Cape Hatteras.

[36] Over the last four decades, three low-salinity events (or Great Salinity Anomaly, GSA) occurred in the Labrador Sea [*Belkin et al.*, 1998; *Dickson et al.*, 1988]. These events, attributed to THC weakening [*Zhang and Vallis*, 2006], illustrate the potential of Labrador Sea salinity to oscillate in response to climate forcing. However, three lines of evidence argue against mechanism 1. A slowdown of the THC is believed to have occurred around 5 ka [*McManus et al.*, 2004], which would lower the salinity in the Labrador Sea according to 'GSA-like' interaction. δ^{18}O measurements over the Laurentian Fan indicates, if anything, a decrease in salinity around 5–3.5 ka (lighter δ^{18}O and no temperature change) [*Keigwin et al.*, 2005]. Finally, a low salinity event was recorded in the Orphan Knoll region around 5–3.5 ka [*Solignac et al.*, 2004]. We see a salinity increase of the Labrador Sea (and therefore Labrador Current) as an explanation for the salinity increase off Cape Hatteras rather unlikely.

[37] We are more confident that mechanism 2 (Labrador Current not reaching Cape Hatteras) explains the surface salinity increase and the less stratified water column between 5.2 and 3.5 ka. According to modern observations, the total latitudinal range of the Gulf Stream path, close to the separation point, is about half a degree [*Gangopadhyay et al.*, 1992]. The Gulf Stream position can shift to the north and block the southward flowing water. Next, we explore two scenarios, possibly related to each other, which explain a northward shift of the Gulf Stream.

[38] 1. The Deep Western Boundary Current (DWBC) is part of the lower limb of the THC: it is the deep counterpart of the Labrador Current. The DWBC flows to the south at the bottom of the western North Atlantic margin: intense recirculation and eddies form when the DWBC meet the Gulf Stream. A reduction of the THC and weakening of the DWBC shift the Gulf Stream path to the north [*Spall*, 1996; *Thompson and Schmitz*, 1989; *Zhang and Vallis*, 2007]. The period 5.2–3.5 ka encompasses known THC change [*Oppo et al.*, 2003] along with a major reorganization of the North Atlantic circulation and deep-water formation [*Andersen et al.*, 2004; *Colin et al.*, 2010; *Hillaire-Marcel et al.*, 2001]. Therefore, a possible scenario for our results is that a weakening of the THC and the DWBC allowed the Gulf Stream to have a more northerly path, diminishing the influence of the Labrador Current at Cape Hatteras.

[39] 2. The absence of Labrador Water off Cape Hatteras may also come from altered atmospheric circulation. Today, the Labrador Current export to the south seems related to negative NAO context [*Marsh*, 2000] or southward blowing wind over the northeastern U.S. coast [*Gawarkiewicz and Linder*, 2006]. The position of the Gulf Stream is also known to move northward with positive NAO condition and southward with a negative phase [*Joyce et al.*, 2000]. As for the deep-ocean, the atmospheric conditions also changed markedly around 5 ka: North African climate shifted abruptly to arid conditions [*deMenocal et al.*, 2000], a large portion of North America experienced mega-drought [*Booth et al.*, 2005], and the Trade winds weakened [*Kim et al.*, 2007]. The second hypothesis is that long lasting NAO-positive-like condition around 5.2–3.5 ka would push the

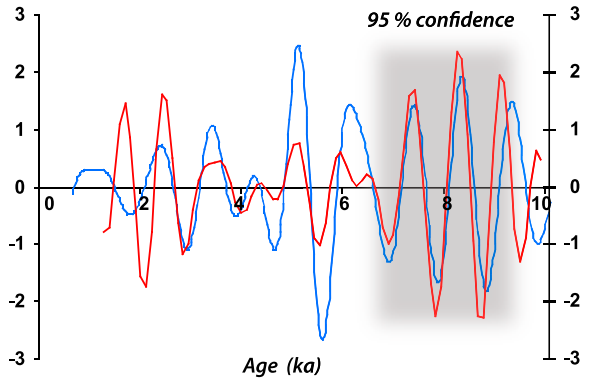

Figure 10. Normalized wavelet 1000-year frequency band for total solar irradiance (TSI) in red [*Steinhilber et al.*, 2009] and *G. ruber* δ^{18}O of MD99-2203 in blue. For each curve, 1000-year frequency band was extracted and plotted on their independent model age. Over the period 9.5−7 ka, the two signals are correlated at 95% confidence (gray area). After 7 ka, the peaks are in phase but the amplitudes are different. In response to an isotopic event around 5 ka in the MD99-2203 record, the wavelet analysis artificially creates the two large amplitude excursions. Note the reduced amplitude of the 1000-year frequency power in TSI between 7 ka and 3 ka.

Gulf Stream path northward; however this contradicts with the Trade wind intensity off Africa [*Kim et al.*, 2007].

[40] On millennial time scales the atmospheric and thermohaline circulation must be considered together and both the wind-forcing and the THC may interact with each other to control the Gulf Stream position. Recently, *Joyce and Zhang* [2010] simulated the Gulf Stream position under various MOC strengths. They showed a more southerly position when MOC is strong and a shift to the north with a weak MOC. We propose that, in response to altered MOC, the Gulf Stream was shifted to the north around 5.2–3.5 ka, and it dammed the export of low salinity Labrador water to the south, resulting in a salinity increase off Cape Hatteras. It is possible that the salinity increase around 8 ka has the same origin. Unfortunately, the Bahamas record starts after this event, and the 'true' Gulf Stream conditions are therefore unknown at 8 ka.

4.3. Solar Variability Signal in the Stable Oxygen Isotopic Record

[41] The 1000-year cycle evidenced by wavelet analysis over the early Holocene in the δ^{18}O record has already been found in a growing number of Holocene reconstructions: all across the Atlantic Ocean [*Chapman and Shackleton*, 2000; *Debret et al.*, 2007], off Baja California [*Marchitto et al.*, 2010], in the Santa Barbara Basin [*Nederbragt and Thurowa*, 2005], in terrestrial North America records [*Chapman and Shackleton*, 2000; *Debret et al.*, 2009; *Nederbragt and Thurowa*, 2005; *Viau et al.*, 2006] or ices cores [*Debret et al.*, 2009]. Since the first work of *Bond et al.* [1997], this millennial scale climate variability has been attributed to solar variability. The amount of incoming solar electromagnetic energy measured at 1 astronomical unit (mean sun–Earth distance) outside of the Earth's atmosphere is the total solar irradiance (TSI). Prior to sunspot observations, solar variability reconstructions are based on cosmogenic radionuclides such as ^{10}Be. ^{10}Be is produced by nuclear reactions between cosmic ray particles and atmospheric gases. After corrections from magnetic field variation, ^{10}Be flux in ice sheet is a proxy for solar activity. To further show the correlation between the surface condition off Cape Hatteras and the sun variability, we compare our *G. ruber* δ^{18}O with TSI reconstruction over the last 9.3 ka [*Steinhilber et al.*, 2009] (Figure 10). Over the last 10 ka, the 1000-year frequency bands of both signals correlate well, and they are statistically significant (95% confidence limit) between 9.5 ka and 7 ka. Our signal is also very well correlated with SST reconstructions off Baja California Sur [*Marchitto et al.*, 2010], as well as with the other signals included in the Marchitto et al. study (figure not shown). The strong correlation between the surface water variability off Cape Hatteras and the solar activity support the idea that climate is responding to small TSI changes (TSI varied by about 2 Wm^{-2} over the last 9.3 ka [*Steinhilber et al.*, 2009]). Using a coupled ocean–atmosphere General Circulation Model, *Swingedouw et al.* [2011] proposed a decadal feedback mechanism to explain the link between solar irradiance and NAO. It involves an oceanic latent heat flux response to radiation variability in the tropics; this in turn affects the transport of temperature anomalies by the Pacific subtropical gyre and the ITCZ position to finally modify the northern hemisphere winds and therefore the NAO. *Marchitto et al.* [2010] also suggest a prominent role for the Pacific Ocean in recording and amplifying solar radiation forcing.

[42] As in most other works [*Debret et al.*, 2009; *Marchitto et al.*, 2010], the 1000-year cycle observed in our record is only clearly identifiable in the early Holocene and seems to disappear afterward. Regarding our records, we cannot exclude, for the most recent part of the Holocene (after 4 ka), that the age model does not impair spectral analysis. After 4 ka, the polynomial equation used for the model age may introduce an uncertainty of about 250 years which may blur the 1000-year cycle. Several hypotheses have been put forward to explain the disappearance of the 1000-year cycle in climate archive. It is worth noting that the power of the 1000-year cycle in TSI reconstruction is not significant after 6 ka (Figure 10), which may explain simply why this frequency was not well transmitted in the climate over this period. It has also been proposed that the solar frequency observed during the early and mid-Holocene is obscured by a thermohaline circulation forcing over the most recent part of the Holocene [*Debret et al.*, 2009; *Stone and Fritz*, 2006]. The large oceanic reorganization in the mid-Holocene, discussed in the previous paragraph, supports this hypothesis. The numerical conceptual model of *Dima and Lohmann* [2009] confirms that the threshold response of the thermohaline circulation to the solar forcing may explain the millennial cycle observed in climate archives. We propose a third hypothesis in light of the amplifier mechanism proposed by *Swingedouw et al.* [2011]. In this mechanism, ITCZ displacement, driven by tropical Pacific SST anomalies, stimulates the atmospheric convection. If the ITCZ plays a role in transmitting the solar-sourced signal in the ocean, large scale ITCZ movement may have then impacted

this feedback. Titanium measurement in the Cariaco Basin indicates a southward displacement of the ITCZ since 8 ka, with a larger step around 5 ka [*Haug et al.*, 2001]. This ITCZ shift may explain a change in the climate response to solar-sourced forcing. A model study will be necessary to test the amplifying mechanism of *Swingedouw et al.* [2011] with a different mean position of the ITCZ.

5. Conclusions

[43] Cape Hatteras, at the Gulf Stream and Labrador Current confluence, is an oceanic region sensitive to both the oceanic and atmospheric forcing. High-resolution SST and salinity reconstructions over the Holocene are studied in the North Atlantic climate context, at the local scale (Gulf Stream variability), and finally the periodic signal is extracted.

[44] Present-day conditions in the Gulf Stream are highly influenced by the NAO and the state of the STG. We qualitatively compared our reconstructions with subsurface temperature and salinity signals in the NE North Atlantic and observed a broad anti-correlation. More than the NAO atmospheric mechanism, we argue that this reflect STG and SPG co-variation. Between 8 and 6.5 ka and 2–1 ka, both gyres show sign of enhanced circulation.

[45] The periods around 8 ka and 5.2–3.5 ka are remarkable with high salinities that are not accompanied with high temperatures. We show that the latter period correspond to an interruption in the low-salinity Labrador Current / Slope Water influence off Cape Hatteras. We examine different scenarios to explain this interruption and suggest that the Gulf Stream was shifted northward and blocked the low salinity southward flowing water, possibly in response to the MOC perturbation recorded around this time.

[46] Wavelet transform analyses on our signals highlight a 1000-year cycle pacing the $\delta^{18}O$ signal from 10 ka to 5.8 ka. This 1000-year cycle previously identified as solar-driven is indeed significantly correlated to TSI reconstruction in the early part of the Holocene. After about 6 ka, the 1000-year cycle disappears; a reduced 1000-year power in TSI cycle, the mid-Holocene THC re-organization, or ITCZ shift may explain a different sensitivity of the climate to solar forcing.

[47] Most of the hypotheses put forward in this paper to explain the observation are based on present-day climate observation or model output. They would need to be tested with other paleoclimate reconstructions or high-resolution (eddy-permitted) model experiments.

[48] **Acknowledgments.** We thank IFREMER, IPEV, IMAGES program, and the *Marion Dufresne* crew for technical support and collection of the core MD99-2203. David Thornalley kindly sent the data for the core RAPiD-12-1K. Great thanks go to Hélène Rebaubier and Gulay Isguder for technical support during geochemical analyses and to Jessica Tierney and Janet Fang for proofreading this manuscript. We send a great thanks to Brad Rosenheim for reviewing this paper and helping with error calculation. Insightful comments from R. Zahn and two other anonymous reviewers greatly improved the overall quality of the manuscript. This work is part of C.C.'s PhD thesis and was supported by a French Research Ministry fellowship. Basic support from CEA and CNRS to the LSCE Paleocean group are acknowledged.

References

Alley, R. B., P. A. Mayewski, M. Sowers, M. Stuiver, K. C. Taylor, and P. U. Clark (1997), Holocene climatic instability: A prominent, widespread event 8200 years ago, *Geology*, *25*, 483–486, doi:10.1130/0091-7613(1997)025<0483:HCIAPW>2.3.CO;2.

Anand, P., H. Elderfield, and M. H. Conte (2003), Calibration of Mg/Ca thermometry in planktonic foraminiferal from a sediment trap series, *Paleoceanography*, *18*(2), 1050, doi:10.1029/2002PA000846.

Andersen, C., N. Koc, A. Jennings, and J. T. Andrews (2004), Nonuniform response of the major surface currents in the Nordic Seas to insolation forcing: Implications for the Holocene climate variability, *Paleoceanography*, *19*, PA2003, doi:10.1029/2002PA000873.

Andersson, C., F. S. R. Pausata, E. J. Jansen, B. Risebrobakken, and R. J. Telford (2010), Holocene trends in the foraminifer record from the Norwegian Sea and the North Atlantic Ocean, *Clim. Past*, *6*, 179–193, doi:10.5194/cp-6-179-2010.

Arbuszewski, J. J., P. B. deMenocal, A. Kaplan, and C. E. Farmer (2010), On the fidelity of shell-derived δ18Oseawater estimates, *Earth Planet. Sci. Lett.*, *300*(3–4), 185–196, doi:10.1016/j.epsl.2010.10.035.

Atkinson, L. P., T. N. Lee, J. O. Blanton, and W. S. Chandler (1983), Climatology of the Southeastern United States Continental Shelf Waters, *J. Geophys. Res.*, *88*(C8), 4705–4718, doi:10.1029/JC088iC08p04705.

Barker, S., M. Greaves, and H. Elderfield (2003), A study of cleaning procedures used for foraminiferal Mg/Ca paleothermometry, *Geochem. Geophys. Geosyst.*, *4*(9), 8407, doi:10.1029/2003GC000559.

Belkin, I. M., S. Levitus, J. Antonov, and S.-A. Malmberg (1998), "Great Salinity Anomalies" in the North Atlantic, *Prog. Oceanogr.*, *41*(1), 1–68, doi:10.1016/S0079-6611(98)00015-9.

Birks, C. J. A., and N. Koç (2002), A high-resolution diatom record of late-Quaternary sea-surface temperatures and oceanographic conditions from the eastern Norwegian Sea, *Boreas*, *31*(4), 323–344, doi:10.1111/j.1502-3885.2002.tb01077.x.

Bond, G., W. Showers, M. Cheseby, R. Lotti, P. Almasi, P. B. deMenocal, P. Priore, H. Cullen, I. Hajdas, and G. Bonani (1997), A pervasive Millenial-Scale cycle in North Atlantic holocene and glacial climates, *Science*, *278*, 1257–1266, doi:10.1126/science.278.5341.1257.

Böning, C. W., M. Scheinert, J. Dengg, A. Biastoch, and A. Funk (2006), Decadal variability of subpolar gyre transport and its reverberation in the North Atlantic overturning, *Geophys. Res. Lett.*, *33*, L21S01, doi:10.1029/2006GL026906.

Booth, R. K., S. T. Jackson, S. L. Forman, J. E. Kutzbach, E. A. I. Bettis, J. Kreigs, and D. K. Wright (2005), A severe centennial-scale drought in midcontinental North America 4200 years ago and apparent global linkages, *Holocene*, *15*(3), 321–328, doi:10.1191/0959683605hl825ft.

Bumpus, D. F. (1973), A description of the circulation on the continental shelf of the east coast of the United States, *Prog. Oceanogr.*, *6*, 111–157, doi:10.1016/0079-6611(73)90006-2.

Came, R., D. W. Oppo, and J. F. McManus (2007), Amplitude and timing of temperature and salinity variability in the subpolar North Atlantic over the past 10 k.y, *Geology*, *35*(4), 315–318, doi:10.1130/G23455A.1.

Chapman, M. R., and N. J. Shackleton (2000), Evidence of 550-year and 1000-year cyclicities in North Atlantic circulation patterns during the Holocene, *Holocene*, *10*(3), 287–291, doi:10.1191/095968300671253196.

Cléroux, C., E. Cortijo, J. C. Duplessy, and R. Zahn (2007), Deep-dwelling foraminifera as thermocline temperature recorders, *Geochem. Geophys. Geosyst.*, *8*, Q04N11, doi:10.1029/2006GC001474.

Cléroux, C., E. Cortijo, P. Anand, L. Labeyrie, F. Bassinot, N. Caillon, and J.-C. Duplessy (2008), Mg/Ca and Sr/Ca ratios in planktonic foraminifera: Proxies for upper water column temperature reconstruction, *Paleoceanography*, *23*, PA3214, doi:10.1029/2007PA001505.

Colin, C., N. Frank, K. Copard, and E. Douville (2010), Neodymium isotopic composition of deep-sea corals from the NE Atlantic: Implications for past hydrological changes during the Holocene, *Quat. Sci. Rev.*, *29*, 2509–2517, doi:10.1016/j.quascirev.2010.05.012.

Conkright, M. E., R. A. Locarnini, H. E. Garcia, T. D. O'Brien, T. P. Boyer, C. Stephens, and J. I. Antonov (2002), *World Ocean Atlas 2001: Objective Analyses, Data Statistics, and Figures* [CD-ROM], 17 pp., NOAA, Silver Spring, Md.

Curry, R. G., and M. S. McCartney (2001), Ocean Gyre Circulation Changes Associated with the North Atlantic Oscillation, *J. Phys. Oceanogr.*, *31*, 3374–3400, doi:10.1175/1520-0485(2001)031<3374:OGCCAW>2.0.CO;2.

Curry, R. G., M. S. McCartney, and T. M. Joyce (1998), Oceanic transport of subpolar signals to mid-depth subtropical waters, *Nature*, *391*, 575–577, doi:10.1038/35356.

Debret, M., V. Bout-Roumazeilles, F. Grousset, M. Desmet, J. F. McManus, N. Massei, D. Sebag, J. R. Petit, Y. Copard, and A. Trentesaux (2007), The origin of the 1500-year climate cycles in Holocene North-Atlantic records, *Clim. Past*, *3*, 569–575, doi:10.5194/cp-3-569-2007.

Debret, M., D. Sebag, X. Crosta, N. Massei, J.-R. Petit, E. Chapron, and V. Bout-Roumazeilles (2009), Evidence from wavelet analysis for a mid-Holocene transition in global climate forcing, *Quat. Sci. Rev.*, *28*, 2675–2688, doi:10.1016/j.quascirev.2009.06.005.

de Coëtlogon, G., C. Frankignoul, M. Bentsen, C. Delon, H. Haak, S. Masina, and A. Pardaens (2006), Gulf Stream variability in five oceanic general circulation models, *J. Phys. Oceanogr.*, *36*(11), 2119–2135, doi:10.1175/JPO2963.1.

deMenocal, P. B., J. D. Ortiz, T. Guilderson, J. Adkins, M. Sarnthein, L. Baker, and M. Yarusinsky (2000), Abrupt onset and termination of the African Humid Period: Rapid climate responses to gradual insolation forcing, *Quat. Sci. Rev.*, *19*, 347–361, doi:10.1016/S0277-3791(99)00081-5.

Dengg, J., A. Beckmann, and R. Gerdes (1996), The Gulf Stream separation problem, in *The Warmwatersphere of the North Atlantic Ocean*, edited by W. Krauss, pp. 253–290, Borntraeger, Berlin.

Deuser, W. G., and E. H. Ross (1989), Seasonally abundant planktonic foraminifera of the Sargasso Sea: Succession, deep-water fluxes, isotopic composition and paleoceanographic implication, *J. Foraminiferal Res.*, *19*, 268–293, doi:10.2113/gsjfr.19.4.268.

Deuser, W. G., E. H. Ross, C. Hemleben, and M. Spindler (1981), Seasonal changes in species composition, numbers, mass, size, and isotopic composition of planktonic foraminifera settling into the deep Sargasso Sea, *Palaeogeogr. Palaeoclimatol. Palaeoecol.*, *33*, 103–127, doi:10.1016/0031-0182(81)90034-1.

Dickson, R. R., J. Meincke, S.-A. Malmberg, and A. J. Lee (1988), The "Great Salinity Anomaly" in the Northern North Atlantic 1968–1982, *Prog. Oceanogr.*, *20*, 103–151, doi:10.1016/0079-6611(88)90049-3.

Dima, M., and G. Lohmann (2009), Conceptual model for millennial climate variability: A possible combined solar-thermohaline circulation origin for the ~1,500-year cycle, *Clim. Dyn.*, *32*, 301–311, doi:10.1007/s00382-008-0471-x.

Dong, B., and R. T. Sutton (2005), Mechanism of Interdecadal Thermohaline Circulation Variability in a Coupled Ocean–Atmosphere GCM, *J. Clim.*, *18*(8), 1117–1135, doi:10.1175/JCLI3328.1.

Elderfield, H., and G. Ganssen (2000), Past temperature and $\delta^{18}O$ of surface ocean waters inferred from foraminiferal Mg/Ca ratios, *Nature*, *405*, 442–445, doi:10.1038/35013033.

Emiliani, C. (1955), Pleistocene temperature, *J. Geol.*, *63*, 538–578, doi:10.1086/626295.

Farmer, E. C., A. Kaplan, P. B. de Menocal, and J. Lynch-Stieglitz (2007), Corroborating ecological depth preferences of planktonic foraminifera in the tropical Atlantic with the stable oxygen isotope ratios of core top specimens, *Paleoceanography*, *22*, PA3205, doi:10.1029/2006PA001361.

Ferguson, J. E., G. M. Henderson, M. Kucera, and R. E. M. Rickaby (2008), Systematic change of foraminiferal Mg/Ca ratios across a strong salinity gradient, *Earth Planet. Sci. Lett.*, *265*(1–2), 153–166, doi:10.1016/j.epsl.2007.10.011.

Frankignoul, C., G. de Coëtlogon, T. M. Joyce, and S. Dong (2001), Gulf Stream variability and ocean-atmosphere interactions, *J. Phys. Oceanogr.*, *31*, 3516–3529, doi:10.1175/1520-0485(2002)031<3516:GSVAOA>2.0.CO;2.

Gangopadhyay, A., P. C. Cornillon, and D. R. Watts (1992), A test of the Parsons-Veronis hypothesis on the separation of the Gulf Stream, *J. Phys. Oceanogr.*, *22*, 1286–1301, doi:10.1175/1520-0485(1992)022<1286:ATOTPH>2.0.CO;2.

Ganssen, G., and D. Kroon (2000), The isotopic signature of planktonic foraminifera from NE Atlantic surface sediments: Implications for the reconstruction of past oceanic conditions, *J. Geol. Soc.*, *157*, 693–699, doi:10.1144/jgs.157.3.693.

Gao, Y.-Q., and L. Yu (2008), Subpolar gyre index and the North Atlantic meridional overturning circulation in a coupled climate model, *Atmos. Oceanic Sci. Lett.*, *1*(1), 29–32.

Gawarkiewicz, G., and C. A. Linder (2006), Lagrangian flow patterns north of Cape Hatteras using near-surface drifters, *Prog. Oceanogr.*, *70*, 181–195, doi:10.1016/j.pocean.2006.03.020.

Giraudeau, J., M. Grelaud, S. Solignac, J. T. Andrews, M. Moros, and E. J. Jansen (2010), Millennial-scale variability in Atlantic water advection to the Nordic Seas derived from Holocene coccolith concentration records, *Quat. Sci. Rev.*, *29*, 1276–1287, doi:10.1016/j.quascirev.2010.02.014.

Gray, S. T., L. J. Graumlich, J. L. Betancourt, and G. T. Pederson (2004), A tree-ring based reconstruction of the Atlantic Multidecadal Oscillation since 1567 A.D, *Geophys. Res. Lett.*, *31*, L12205, doi:10.1029/2004GL019932.

Halliwell, G. R. J. (1998), Simulation of North Atlantic decadal/multidecadal winter SST anomalies driven by basin-scale atmospheric circulation anomalies, *J. Phys. Oceanogr.*, *28*, 5–21, doi:10.1175/1520-0485(1998)028<0005:SONADM>2.0.CO;2.

Hatun, H., A. B. Sandro, H. Drange, B. Hansen, and H. Valdimarsson (2005), Influence of the Atlantic subpolar gyre on the thermohaline circulation, *Science*, *309*, 1841–1844, doi:10.1126/science.1114777.

Haug, G. H., K. Hughen, D. M. Sigman, L. Peterson, and U. Röhl (2001), Southward migration of the Intertropical Convergence Zone through the Holocene, *Science*, *293*, 1304–1308, doi:10.1126/science.1059725.

Hillaire-Marcel, C., A. de Vernal, G. Bilodeau, and A. J. Weaver (2001), Absence of deep-water formation in the Labrador Sea during the last interglacial period, *Nature*, *410*, 1073–1077, doi:10.1038/35074059.

Hurrell, J. W., Y. Kushnir, G. Ottersen, and M. Visbeck (2003), An overview of the North Atlantic Oscillation, in *The North Atlantic Oscillation: Climatic Significance and Environmental Impact*, *Geophys. Monogr. Ser.*, vol. 134, edited by J. W. Hurrell et al., pp. 1–35, AGU, Washington, D. C., doi:10.1029/134GM01.

Joyce, T. M., and R. Zhang (2010), On the Path of the Gulf Stream and the Atlantic Meridional Overturning Circulation, *J. Clim.*, *23*(11), 3146–3154, doi:10.1175/2010JCLI3310.1.

Joyce, T. M., C. Deser, and M. Spall (2000), The relation between Decadal Varability of Subtropical Mode Water and the North Atlantic Oscillation, *J. Clim.*, *13*(14), 2550–2569, doi:10.1175/1520-0442(2000)013<2550:TRBDVO>2.0.CO;2.

Keigwin, L. D., J. P. Sachs, Y. Rosenthal, and E. A. Boyle (2005), The 8200 year B.P. event in the slope water system, western subpolar North Atlantic, *Paleoceanography*, *20*, PA2003, doi:10.1029/2004PA001074.

Kelly, K. A., and S. Dong (2004), The relationship of western boundary current heat transport and storage to midlatitude ocean-atmosphere interaction, in *Earth's Climate: The Ocean-Atmosphere Interaction*, *Geophys. Monogr. Ser.*, vol. 147, edited by C. Wang, S.-P. Xie, and J. A. Carton, pp. 347–363, AGU, Washington, D. C., doi:10.1029/147GM19.

Kim, J.-H., H. Meggers, N. Rimbu, G. Lohmann, T. Freudenthal, P. J. Müller, and R. Schneider (2007), Impacts of the North Atlantic gyre circulation on Holocene climate off northwest Africa, *Geology*, *35*(5), 387–390, doi:10.1130/G23251A.1.

Kleiven, H. F., C. Kissel, C. Laj, U. S. Ninnemann, T. O. Richter, and E. Cortijo (2008), Reduced North Atlantic Deep Water coeval with the Glacial Lake Agassiz freshwater outburst, *Science*, *319*, 60–64, doi:10.1126/science.1148924.

Knudsen, M. F., P. Riisager, B. H. Jacobsen, R. Muscheler, I. Snowball, and M.-S. Seidenkrantz (2009), Taking the pulse of the Sun during the Holocene by joint analysis of ^{14}C and ^{10}Be, *Geophys. Res. Lett.*, *36*, L16701, doi:10.1029/2009GL039439.

Laskar, J. (1990), The chaotic motion of the solar system - A numerical estimate of the size of the chaotic zones, *Icarus*, *88*, 266–291, doi:10.1016/0019-1035(90)90084-M.

Laskar, J., P. Robutel, F. Joutel, M. Gastineau, A. C. M. Correia, and B. Levrard (2004), A long-term numerical solution for the insolation quantities of the Earth, *Astron. Astrophys.*, *428*(1), 261–285, doi:10.1051/0004-6361:20041335.

Latif, M., C. Böning, J. Willebrand, A. Biastoch, M. Dengg, N. Keenlyside, U. Schweckendiek, and G. Madec (2006), Is the thermohaline circulation changing?, *J. Clim.*, *19*, 4631–4637, doi:10.1175/JCLI3876.1.

Lohmann, G., N. Rimbu, and M. Dima (2004), Climate signature of solar irradiance variations: Analysis of long-term instrumental, historical, and proxy data, *Int. J. Climatol.*, *24*(8), 1045–1056, doi:10.1002/joc.1054.

Lohmann, K., H. Drange, and M. Bentsen (2009), Response of the North Atlantic subpolar gyre to persistent North Atlantic oscillation like forcing, *Clim. Dyn.*, *32*, 273–285, doi:10.1007/s00382-008-0467-6.

Lund, D. C., and W. B. Curry (2006), Florida current surface temperature and salinity variability during the last millennium, *Paleoceanography*, *21*, PA2009, doi:10.1029/2005PA001218.

Marchitto, T. M., R. Muscheler, J. D. Ortiz, J. D. Carriquiry, and A. van Geen (2010), Dynamical response of the tropical Pacific Ocean to solar forcing during the Early Holocene, *Science*, *330*, 1378–1381, doi:10.1126/science.1194887.

Marsh, R. (2000), Recent variability of the North Atlantic thermohaline circulation inferred from surface heat and freshwater fluxes, *J. Clim.*, *13*, 3239–3260, doi:10.1175/1520-0442(2000)013<3239:RVOTNA>2.0.CO;2.

Marshall, J., H. Johnson, and J. Goodman (2001), A Study of the Interaction of the North Atlantic Oscillation with Ocean Circulation, *J. Clim.*, *14*, 1399–1421, doi:10.1175/1520-0442(2001)014<1399:ASOTIO>2.0.CO;2.

Mathien-Blard, E., and F. Bassinot (2010), Salinity bias on the foraminifera Mg/Ca thermometry: Correction procedure and implications for past ocean hydrographic reconstructions, *Geochem. Geophys. Geosyst.*, *10*, Q12011, doi:10.1029/2008GC002353.

McManus, J. F., R. François, J.-M. Gherardi, L. D. Keigwin, and S. Brown-Leger (2004), Collapse and rapid resumption of atlantic meridional circulation linked to deglacial climate changes, *Nature*, *428*, 834–837, doi:10.1038/nature02494.

Morley, A., M. Schulz, Y. Rosenthal, S. Mulitza, A. Paul, and C. Rühlemann (2011), Solar modulation of North Atlantic central Water formation at multidecadal timescales during the late Holocene, *Earth Planet. Sci. Lett.*, *308*, 161–171, doi:10.1016/j.epsl.2011.05.043.

Nederbragt, A. J., and J. Thurowa (2005), Geographic coherence of millennial-scale climate cycles during the Holocene, *Palaeogeogr. Palaeoclimatol. Palaeoecol.*, *221*(3–4), 313–324, doi:10.1016/j.palaeo.2005.03.002.

Nürnberg, D., J. Bijma, and C. Hemleben (1996), Assessing the reliability of magnesium in foraminiferal calcite as a proxy for water mass temperatures, *Geochim. Cosmochim. Acta*, *60*(5), 803–814, doi:10.1016/0016-7037(95)00446-7.

Oppo, D. W., J. F. McManus, and J. L. Cullen (2003), Palaeo-oceanography: Deepwater variability in the Holocene epoch, *Nature*, *422*, 277, doi:10.1038/422277b.

Pietrafesa, L., J. M. Morrison, M. P. McCann, J. Churchill, E. Böhm, and R. W. Houghton (1994), Water mass linkages between the Middle and South Atlantic Bights, *Deep Sea Res., Part II*, *41*, 365–389, doi:10.1016/0967-0645(94)90028-0.

Rimbu, N., G. Lohmann, J.-H. Kim, H. W. Arz, and R. Schneider (2003), Arctic/North Atlantic Oscillation signature in Holocene sea surface temperature trends as obtained from alkenone data, *Geophys. Res. Lett.*, *30*(6), 1280, doi:10.1029/2002GL016570.

Rimbu, N., G. P. Lohmann, S. J. Lorenz, J.-H. Kim, and R. Schneider (2004), Holocene climate variability as derived from alkenone sea surface temperature and coupled ocean-atmophere model experiment, *Clim. Dyn.*, *23*, 215–227, doi:10.1007/s00382-004-0435-8.

Risebrobakken, B., E. J. Jansen, C. Andersson, E. Mjelde, and K. Hevroy (2003), A high-resolution study of Holocene paleoclimatic and paleoceanographic changes in the Nordic Seas, *Paleoceanography*, *18*(1), 1017, doi:10.1029/2002PA000764.

Roth, S., and J. J. G. Reijmer (2004), Holocene Atlantic climate variations deduced from carbonate periplatform sediments (leeward margin, Great Bahama Bank), *Paleoceanography*, *19*, PA1003, doi:10.1029/2003PA000885.

Rozanski, K., L. Araguás-Araguás, and R. Gonfiantini (1993), Isotopic patterns in modern global precipitation, in *Climate Change in Continental Isotopic Records*, *Geophys. Monogr. Ser.*, vol. 78, edited by P. K. Swart et al., pp. 1–36, AGU, Washington, D. C., doi:10.1029/GM078p0001.

Saenger, C., A. L. Cohen, D. W. Oppo, R. B. Halley, and J. E. Carilli (2009), Surface-temperature trends and variability in the low-latitude North Atlantic since 1552, *Nat. Geosci.*, *2*, 492–495, doi:10.1038/ngeo552.

Schmidt, G. A. (1999), Error analysis of paleosalinity calculations, *Paleoceanography*, *14*(3), 422–429, doi:10.1029/1999PA900008.

Schmidt, G. A., G. R. Bigg, and E. J. Rohlin (1999), Global Seawater Oxygen-18 Database, http://data.giss.nasa.gov/o18data/, NASA Goddard Space Flight Cent., Greenbelt, Md.

Schmidt, G. A., A. N. LeGrande, and G. Hoffmann (2007), Water isotope expressions of intrinsic and forced variability in a coupled ocean-atmosphere model, *J. Geophys. Res.*, *112*, D10103, doi:10.1029/2006JD007781.

Schmitz, W. J. J., and M. S. McCartney (1993), On the North Atlantic circulation, *Rev. Geophys.*, *31*(1), 29–49, doi:10.1029/92RG02583.

Shackleton, N. J. (1974), Attainment of isotopic equilibrium between ocean water and benthonic foraminifera genus Uvigerina: Isotopic changes in the ocean during the last glacial, *Cent. Nat. Res., Sci. Colloq. Int.*, *219*, 203–209.

Sicre, M.-A., P. Yiou, J. Eiriksson, U. Ezat, E. Guimbaut, I. Dahhaoui, K.-L. Knudsen, E. Jansen, and J.-L. Turon (2008), A 4500-year reconstruction of sea surface temperature variability at decadal time-scales off North Iceland, *Quat. Sci. Rev.*, *27*, 2041–2047, doi:10.1016/j.quascirev.2008.08.009.

Solignac, S., A. de Vernal, and C. Hilaire-Marcel (2004), Holocene sea-surface conditions in the North Atlantic—Contrasted trends and regimes in the western and eastern sectors (Labrador Sea vs. Iceland Basin), *Quat. Sci. Rev.*, *23*, 319–334, doi:10.1016/j.quascirev.2003.06.003.

Spall, M. (1996), Dynamics of the Gulf Sream/Deep Western Boundary Current crossover. Part II: Low-frequency internal oscillations, *J. Phys. Oceanogr.*, *26*, 2169–2182, doi:10.1175/1520-0485(1996)026<2169:DOTGSW>2.0.CO;2.

Steinhilber, F., J. Beer, and C. Fröhlich (2009), Total solar irradiance during the Holocene, *Geophys. Res. Lett.*, *36*, L19704, doi:10.1029/2009GL040142.

Steinhilber, F., J. A. Abreu, J. Beer, and K. G. McCracken (2010), Interplanetary magnetic field during the past 9300 years inferred from cosmogenic radionuclides, *J. Geophys. Res.*, *115*, A01104, doi:10.1029/2009JA014193.

Steph, S., M. Regenberg, R. Tiedemann, S. Mulitza, and D. Nürnberg (2009), Stable isotopes of planktonic foraminifera from tropical Atlantic/Caribbean coretops: Implications for reconstructing upper ocean stratification, *Mar. Micropaleontol.*, *71*, 1–19, doi:10.1016/j.marmicro.2008.12.004.

Stephenson, D. B., H. Wanner, S. Brönnimann, and J. Luterbacher (2003), The history of scientific research on the North Atlantic Oscillation, in *The North Atlantic Oscillation: Climatic Significance and Environmental Impact*, *Geophys. Monogr. Ser.*, vol. 134, edited by J. W. Hurrell et al., pp. 37–50, AGU, Washington, D. C., doi:10.1029/134GM02.

Stone, J. R., and S. C. Fritz (2006), Multidecadal drought and Holocene climate instability in the Rocky Mountains, *Geology*, *34*(5), 409–412, doi:10.1130/G22225.1.

Stuiver, M., P. J. Reimer, and E. Bard (1998), INTERCAL98 radiocarbon age calibration, 24 000–0 cal BP, *Radicarbon*, *40*(3), 1041–1083.

Swingedouw, D., L. Terray, C. Cassou, A. Voldoire, D. Salas-Mélia, and J. Servonnat (2011), Natural forcing of climate during the last millennium: Fingerprint of solar variability, *Clim. Dyn.*, *36*, 1349–1364, doi:10.1007/s00382-010-0803-5.

Thacker, W. C. (2007), Estimating salinity to complement observed temperature: 1. Gulf of Mexico, *J. Mar. Syst.*, *65*, 224–248, doi:10.1016/j.jmarsys.2005.06.008.

Thacker, W. C., and L. Sindlinger (2007), Estimating salinity to complement observed temperature: 2. Northwestern Atlantic, *J. Mar. Syst.*, *65*, 249–267, doi:10.1016/j.jmarsys.2005.06.007.

Thomas, E. R., E. W. Wolff, R. Mulvaney, J. P. Steffensen, S. J. Johnsen, C. Arrowsmith, J. W. C. White, B. Vaughn, and T. Popp (2007), The 8.2 ka event from Greenland ice cores, *Quat. Sci. Rev.*, *26*(1–2), 70–81, doi:10.1016/j.quascirev.2006.07.017.

Thompson, J. D., and J. W. J. Schmitz (1989), A limited-area model of the Gulf Stream: Design, initial experiments, and model-data intercomparison, *J. Phys. Oceanogr.*, *19*(6), 791–814, doi:10.1175/1520-0485(1989)019<0791:ALAMOT>2.0.CO;2.

Thornalley, D. J. R., H. Elderfield, and I. N. McCave (2009), Holocene oscillations in temperature and salinity of the surface subpolar North Atlantic, *Nature*, *457*, 711–714, doi:10.1038/nature07717.

Viau, A. E., K. Gajewski, M. C. Sawada, and P. Fines (2006), Millennial-scale temperature variations in North America during the Holocene, *J. Geophys. Res.*, *111*, D09102, doi:10.1029/2005JD006031.

Visbeck, M., J. W. Hurrell, L. Polvani, and H. Cullen (2001), The North Atlantic Oscillation: Past, present, and future, *Proc. Natl. Acad. Sci. U. S. A.*, *98*(23), 12,876–12,877, doi:10.1073/pnas.231391598.

Waelbroeck, C., L. Labeyrie, E. Michel, J. C. Duplessy, J. F. McManus, K. Lambeck, E. Balbon, and M. Labracherie (2002), Sea-level and deep water temperature changes derived from benthic foraminifera isotopic records, *Quat. Sci. Rev.*, *21*, 295–305, doi:10.1016/S0277-3791(01)00101-9.

Wang, Y., H. Cheng, R. L. Edwards, Y. He, X. Kong, Z. An, J. Wu, M. J. Kelly, C. A. Dykoski, and X. Li (2005), The Holocene Asian Monsoon: Links to solar changes and North Atlantic climate, *Science*, *308*, 854–857, doi:10.1126/science.1106296.

Wanner, H., et al. (2008), Mid- to Late Holocene climate change: An overview, *Quat. Sci. Rev.*, *27*, 1791–1828, doi:10.1016/j.quascirev.2008.06.013.

Waple, A., M. E. Mann, and R. Bradley (2002), Long-term patterns of solar irradiance forcing in model experiments and proxy based surface temperature reconstructions, *Clim. Dyn.*, *18*(7), 563–578.

Wiersma, A. P., and H. Renssen (2006), Model–data comparison for the 8.2 ka BP event: Confirmation of a forcing mechanism by catastrophic drainage of Laurentide Lakes, *Quat. Sci. Rev.*, *25*, 63–88, doi:10.1016/j.quascirev.2005.07.009.

Zhang, R., and G. Vallis (2006), Impact of great salinity anomalies on the low-frequency variability of the North Atlantic climate, *J. Clim.*, *19*, 470–482, doi:10.1175/JCLI3623.1.

Zhang, R., and G. K. Vallis (2007), The role of bottom vortex stretching on the path of the North Atlantic Western Boundary Current and on the Northern Recirculation Gyre, *J. Phys. Oceanogr.*, *37*, 2053–2080, doi:10.1175/JPO3102.1.

C. Cléroux, Lamont-Doherty Earth Observatory, Columbia University, 61 Rte. 9W, Palisades, NY 10964, USA. (ccleroux@ldeo.columbia.edu)

E. Cortijo, F. Dewilde, and J.-C. Duplessy, Laboratoire des Sciences du Climat et de l'Environnement, CEA-CNRS-UVSQ/IPSL, F-91198 Gif-sur-Yvette, France.

M. Debret and N. Massei, Laboratoire de Morphodynamique Continentale et Côtière, Département de Géologie, Université de Rouen, UMR CNRS/INSU 6143, F-76821 Mont-Saint-Aignan, CEDEX, France.

J. Reijmer, Department of Sedimentology and Marine Geology, FALW, VU University Amsterdam, NL-1081 HV Amsterdam, Netherlands.